Investigation of the CO_2 Activation and Regeneration of Reduced VO_x/CeO_2 Catalysts Using Multiple In Situ Spectroscopies

Leon Schumacher,[a] Marc Ziemba,[a] and Christian Hess*[a]

Ceria-supported vanadium oxide (VO_x/CeO_2) is an important catalyst for various oxidation reactions. Recently, vanadia has emerged again as a less toxic alternative to CrO_x-based catalysts for the CO_2-assisted oxidative dehydrogenation (ODH) of alkanes. To establish a mechanistic understanding of catalyst regeneration during CO_2 exposure, often described as the rate-limiting step of these reactions, we investigated the regeneration of VO_x/CeO_2 catalysts with different vanadia loadings using multiple in situ spectroscopies, that is, multi-wavelength Raman, UV-Vis, IR and X-ray photoelectron spectroscopy. Time-dependent analysis reveals that ceria is only partially regenerated in the bulk but fully regenerated in the subsurface. At the surface, stable carbonates form at vacancies, which are able to regenerate the lattice and deactivate ceria surface oxygen. The VO_x/CeO_2 samples show a loading-dependent behavior, with low-loaded samples regenerating vanadia only partially, due to the high concentration of monomers, while at higher loadings, vanadia can be almost fully regenerated due to the higher nuclearities being thermodynamically more stable. Ceria is regenerated faster than vanadia, indicating that vanadia regenerates by oxygen spill-over from the ceria lattice. Our results provide important mechanistic insight into CO_2 activation over supported vanadia catalysts, which is of great relevance for CO_2-assisted ODH reactions.

1. Introduction

CO_2 is an undesirable greenhouse gas, which is emitted in many industrial processes and significantly contributes to climate change.[1] One way to reduce emissions is to make carbon-capture more viable by finding uses for abundant CO_2 in industrial processes as a feed gas to produce value-added products while reducing atmospheric CO_2 concentrations,[2–6] including chemical processes like methanol synthesis[7] or CO_2-assisted selective alkane oxidations.[8] The use of CO_2 instead of O_2 can even further improve processes, due to its high heat capacity, leading to a more homogeneous temperature distribution within the reactor and decreasing the flammability of some reactions, thus facilitating the scale-up.[9,10] However, due to its thermodynamic stability the activation of CO_2 requires high temperatures.[11,12] Thus, there is a need for development of suitable catalysts, facilitating the use of CO_2 as oxidizing agent.

An important class of catalysts for oxidation reactions is supported VO_x,[13,14] which is often used in the oxidative dehydrogenation (ODH) of alcohols and short alkanes with O_2 as the oxidizing agent.[15,16] For alkanes, the CO_2-assisted ODH has been shown to be of interest for technical applications, since alkane oxidation requires comparably high temperatures, while alcohols would be fully oxidized at the temperatures required for CO_2 activation.[17–21] In addition, the ODH of short alkanes is of great interest to meet the high and further increasing demand for ethylene and propylene.[22] Regarding CO_2-assisted propane ODH, CrO_x has been intensively investigated due to its high activity.[9,23–26] However, due to the toxicity of chromium a substitution with a different catalyst system is highly desirable.[27] Supported vanadia has recently gained attention as a potential substitute since its activity and properties can be fine-tuned by the choice of the support material, influencing the vanadia structure.[28,29]

One of the most active support materials for vanadia in regard to oxygen mobility is ceria,[30–32] which is also an established material for other reactions requiring CO_2 activation such as the reverse water-gas shift reaction (rWGSR),[33,34] the electro-reduction of CO_2[35] or methanol synthesis.[36,37] As oxygen mobility is a key factor for alkane ODH,[38–41] ceria is a promising vanadia support material for CO_2-assisted propane ODH, but has not been studied for its use in this reaction. The re-oxidation step becomes often rate-limiting in systems with less active supports (e.g. SiO_2 or Al_2O_3), which may lead to insufficient re-oxidation and, as a consequence, to a strong reduction of the catalyst, enabling unselective reaction pathways to occur, such as propane dry reforming (PDR) or cracking, thereby decreasing the propylene yield.[19,25,42–44] Coking can even lead to a full deactivation of the catalyst.[25,42–44] Therefore, understanding and improving the re-oxidation process is highly important to improve CO_2-assisted catalysis. The combination of vanadia and ceria might omit these problems, since CeO_2 is

[a] L. Schumacher, M. Ziemba, C. Hess
Department of Chemistry, Technical University of Darmstadt, Eduard-Zintl-Institut für Anorganische und Physikalische Chemie, Peter-Grünberg-Str. 8, 64287 Darmstadt, Germany
E-mail: christian.hess@tu-darmstadt.de

described as a good CO_2 activator,[45] while vanadia has previously been described to enhance CO_2 activation and re-oxidation while actively participating in the redox cycle during propane ODH on other supports (e.g. In_2O_3).[19,20] However, open questions encompass the nature of the re-oxidation pathways, the role of the ceria support, as well as the dependence on vanadia nuclearity.

This study aims at elucidating the re-oxidation behavior of reduced VO_x/CeO_2 in detail, by combining multiple in situ and quasi in situ methods measured over 16 h during catalyst regeneration. For a detailed understanding of bulk, subsurface and surface processes, we applied multi-wavelength Raman, UV-Vis, X-ray photoelectron and diffuse reflectance IR Fourier transform (DRIFT) spectroscopy. The use of multi-wavelength Raman spectroscopy allows for a dedicated investigation of the ceria support and the active vanadia phase by selective intensity enhancement caused by resonance effects. Our findings provide new mechanistic insight into CO_2 activation over vanadia-based catalysts and establish an experimental basis to understand the re-oxidation process on a molecular level.

Experimental Section

Catalyst Preparation

The ceria support was prepared by two-fold calcination of cerium(III) nitrate hexahydrate ($\geq$ 99.99%, Sigma Aldrich) at 600 °C for 12 h, after heating from room temperature to 600 °C using a rate of 1.5 °C/min, as described previously.[32] The ceria was loaded with vanadia by incipient wetness impregnation. Three different loadings were prepared by mixing 1 g of ceria with 0.5 mL of different-concentration precursor solutions (1.07 mol/L, 0.51 mol/L, and 0.21 mol/L) containing vanadium(V) oxytriisopropoxide ($\geq$ 97%, Sigma Aldrich) and 2-propanol (99.5%, Sigma Aldrich). The specific surface area of bare ceria was determined to be 61.4 m^2/g by nitrogen physisorption experiments and the use of the Brunauer-Emmett-Teller (BET) method, yielding vanadium loadings of 2.83 V/nm^2 (2.32 wt% V_2O_5), 1.36 V/nm^2 (1.11 wt% V_2O_5), and 0.57 V/nm^2 (0.47 wt% V_2O_5), respectively. Higher vanadium loadings were not considered since vanadia crystallites were shown to be present at loadings > 2.9 V/nm^2.[46] The resulting catalyst powders were subsequently pressed at a pressure of 2000 kg/m^2 for 20 s, ground and then sieved using a combination of sieves to obtain 200–300 μm particles.

Gas Treatment

The samples were first dehydrated in 12.5% O_2/He at 365 °C for 1 h. For in situ experiments (UV-Raman, Vis-Raman, UV-Vis), the samples were then heated to 550 °C under the same gas feed (oxidative conditions) and after 30 minutes of equilibration a spectrum was recorded. Consecutive treatments consisted of 7.5% H_2/Ar (reductive conditions) and 12.5% CO_2/He (regenerative conditions) at 550 °C. A spectrum was recorded after 30 minutes of equilibration in H_2, while under CO_2 atmosphere, spectra were recorded after 30, 60, 90, 120, 150, and 960 minutes to follow the regeneration process. For the quasi in situ measurements (XPS, DRIFTS), the same procedure was applied but the samples were cooled down to room temperature in pure helium before spectra were recorded and the

regeneration process was followed only for the first 30 minutes. The total flow rate during all measurements was 40 ml/min.

UV-Raman Spectroscopy

UV-Raman spectroscopy was performed at an excitation wavelength of 385 nm generated by a laser system based on a Ti:Sa solid state laser pumped by a frequency-doubled Nd:YAG laser (Coherent, Indigo). The fundamental wavelength was frequency doubled to 385 nm using a LiB_3O_5 crystal. The light was focused onto the sample, and the scattered light was collected by a confocal mirror setup and focused into a triple-stage spectrometer (Princeton Instruments, TriVista 555).[46] Finally, the Raman contribution was detected by a charge-coupled device (CCD, 2048×512 pixels) cooled to −120 °C. The spectral resolution of the spectrometer was 1 cm^{-1}. For Raman experiments, 70 mg of catalyst was placed in a CCR 1000 reactor (Linkam Scientific Instruments) equipped with a CaF_2 window (Korth Kristalle GmbH). A fluidized bed reactor was employed to avoid laser-induced damage, allowing the use of a laser power of 9 mW at the location of the sample. Data processing included cosmic ray removal and background subtraction. The spectra were further analyzed by a least-squares fitting analysis using four Lorentzian functions (see Figure S6).

Vis-Raman Spectroscopy

Visible (Vis) Raman spectroscopy was performed at 514 nm excitation, emitted from an argon-ion laser (Melles Griot). The light was focused onto the sample, gathered by an optical fiber and dispersed by a transmission spectrometer (Kaiser Optical, HL5R). The dispersed Raman radiation was subsequently detected by an electronically cooled CCD detector (−40 °C, 1024×256 pixels). The spectral resolution was 5 cm^{-1} with a wavelength stability of better than 0.5 cm^{-1}. For Raman experiments, 70 mg of catalyst was filled into a CCR 1000 reactor (Linkam Scientific Instruments) equipped with a quartz window (Linkam Scientific Instruments). The laser power at the sample location was 4 mW. Data analysis of the Raman spectra included a cosmic ray removal and an auto new dark correction. The vanadyl areas were quantified by integration using OriginLab, while the nuclearity distribution was determined by performing a least-square fitting analysis using five Lorentzian functions at distinct spectral positions. The F_{2g} mode was fitted without any positional restrictions due to the possible occurrence of red-shifts.

Diffuse Reflectance UV-Vis Spectroscopy

Diffuse reflectance (DR) UV-Vis spectra were recorded on a Jasco V-770 UV-Vis spectrometer. Dehydrated $BaSO_4$ was used as the white standard. For each experiment, 90 mg of catalyst was put in the commercially available reaction cell (Praying Mantis High Temperature Reaction Chamber, Harrick Scientific) equipped with transparent quartz glass windows. The band gap energies were determined using Tauc plots, while the reduction peak area was quantified by a least square fitting analysis of the spectra using Gaussian-Lorentzian (70/30) product functions to account for the large contribution of natural line broadening (Lorentzian) to the overall line-shape, caused by the short life-time of the electronically excited states.[47]

X-Ray Photoelectron Spectroscopy

X-ray photoelectron (XP) spectra were recorded on a modified LHS/SPECS EA200 MCD system described previously.[48–50] The XPS

ChemCatChem

Research Article
doi.org/10.1002/cctc.202301409

Chemistry Europe
European Chemical
Societies Publishing

system was equipped with a Mg Kα source (1253.6 eV, 168 W); the calibration of the binding energy scale was performed with Au $4f_{7/2} = 84.0$ eV and Cu $2p_{3/2} = 932.67$ eV signals from foil samples. To account for sample charging, the C 1s peak of ubiquitous carbon at 284.4 eV was used to correct the binding energies. Detailed spectra were recorded at a resolution of 0.1 eV. The X-ray satellite peaks due to the use of a non-monochromatic source were subtracted from the spectra. The deconvolutions of the spectra were performed analogously for all measurements using Gauss-Lorentzian product functions (30/70). The background was subtracted by the Shirley method.

For determination of surface compositions, peak areas were corrected with the corresponding relative sensitivity factors, i.e., 10 for the Ce 3d, 0.66 for the O 1s and 1.3 for the V $2p_{3/2}$ signal.[51]

Diffuse Reflectance Infrared Fourier Transform Spectroscopy

DRIFT spectra were recorded on a Vertex 70 spectrometer (Bruker), equipped with a liquid nitrogen-cooled mercury cadmium telluride (MCT) detector, operating at a resolution of 1 cm^{-1}. Dehydrated potassium bromide was used as an infrared transparent sample for the background spectrum. For each experiment, 90 mg of the catalyst was placed in the reaction cell (Praying Mantis High Temperature Reaction Chamber, Harrick Scientific) equipped with transparent KBr windows. Data processing consisted of background removal by subtraction of a baseline formed by 12 anchor points.

2. Results and Discussion

The results of an extensive structural characterization of the same series of samples as used in this study were described previously in detail and include analysis of the specific surface area, XRD analysis, as well as a detailed analysis of the temperature-dependent reduction behavior using multiple in situ spectroscopy analysis, including XPS analysis[41,52,53] Figure 1 shows in situ UV-Vis spectra of bare ceria and the 1.36 V/nm^2 sample at 550 °C under oxidative and reductive conditions, as well as after different times of CO_2 exposure. The band gap energy shifts and the reduction peak area (between 500 and 800 nm) was quantified (see Experimental Section) and is summarized in Figure 1c and d, respectively. The corresponding in situ UV-Vis spectra of the 0.57 and 2.83 V/nm^2 samples are
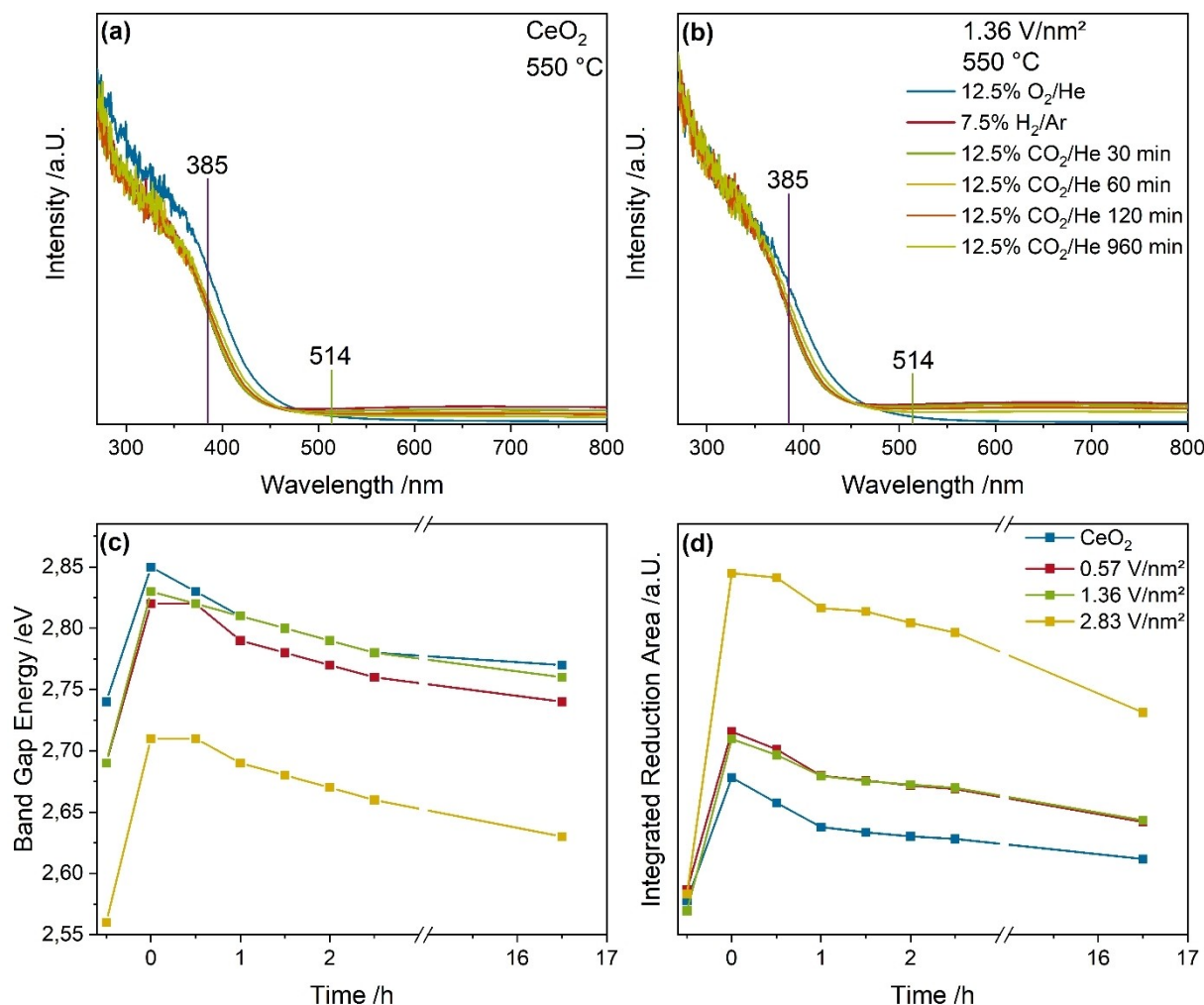
Figure 1. In situ UV-Vis spectra of **(a)** bare CeO_2 and **(b)** the 1.36 V/nm^2 sample recorded under different gas feeds at 550 °C. The used Raman excitation wavelengths are indicated. The **(c)** band gap energy shifts and **(d)** reduction peak area was determined using Tauc plots and a least-square fit analysis (see Experimental Section), respectively.

ChemCatChem

Research Article
doi.org/10.1002/cctc.202301409

Chemistry
Europe
European Chemical
Societies Publishing

given in the SI (see Figure S1). For clarity, the spectra recorded in 12.5% CO_2/He after 90 and 150 minutes are not shown.

Figure 1a shows the UV-Vis spectra of bare ceria. The UV-region is dominated by features at 260 and 330 nm caused by band gap absorption from ceria (O 2p to Ce 4f transitions).[54,55] Raman spectroscopy was performed at the two indicated excitation wavelengths, allowing for selective resonance enhancement of ceria (by using 385 nm excitation) and vanadia (by using 514 nm excitation), as will be discussed below.[41,56] Upon switching from oxidative to reductive conditions, an additional broad band is observed at around 633 nm, which originates from charge transfer from Ce^{3+} to Ce^{4+} indicative of ceria reduction.[57,58] Additionally, during this switch, the band gap energy shows a significant blue-shift. This is notable since ceria reduction typically induces a red-shift caused by the presence of additional reduced states being created in the band gap.[59] However, in addition to the shift, the band around 633 nm, which is indicative of reduced states, increases significantly. Such a behavior was previously observed to blue-shift the apparent band gap determined from Tauc plots due to the additional absorption,[41] and is confirmed under regenerative conditions, where the 633 nm band declines and the band gap gradually red-shifts over time (both indicating re-oxidation).

The UV-Vis spectra of the 1.36 V/nm^2 sample show similar transitions as those of bare ceria (see Figure 1b), indicating the dominance of bulk ceria contributions. These overlap with ligand-to-metal-charge transfer (LMCT) transitions of short-chain vanadia species.[60] Under reductive conditions a very broad additional band around 775 nm, caused by d-d transitions of reduced vanadia states, can overlap with the broad ceria reduction band around 633 nm,[61] leading to an increase in the absorption within 500–800 nm. To better understand the changes of the band gap energy and reduction peak intensity, a quantification using Tauc plots[32] and a least-square fitting procedure (see Experimental Section) was applied, respectively (see Figure 1c and d). Note that in Figure 1c and d, the zero point on the abscissa was shifted to the beginning of the regeneration of the reduced sample with CO_2.
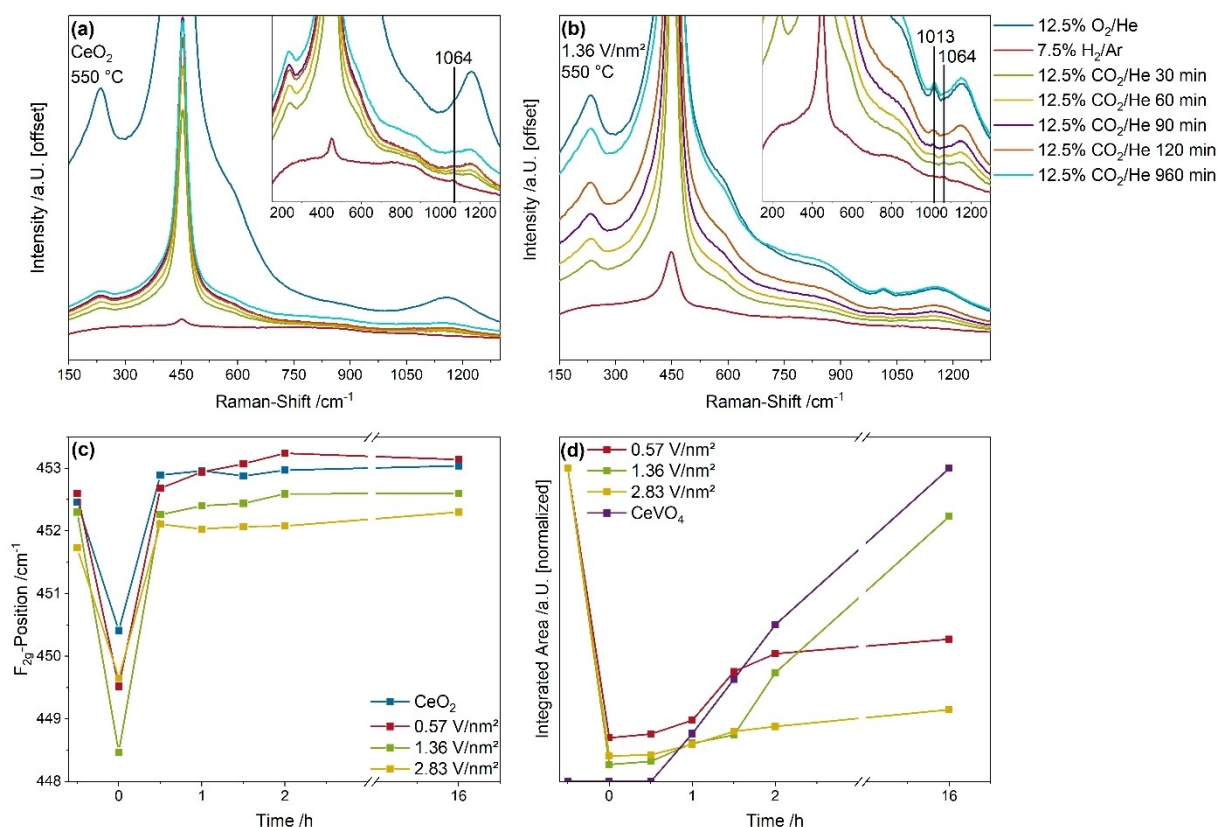
As shown in Figure 1c, the band gap energies for all samples show a similar trend, characterized by a significant blue-shift under reductive conditions and a gradual red-shift during CO_2 exposure. A comparison of band gap energies reveals that bare ceria is characterized by the highest band gap but the lowest shift upon switching from oxidative to reductive conditions, whereas the observed shift increases with increasing vanadium loading. This is in agreement with our previous results on the reduction behavior of the VO_x/CeO_2 samples.[52] The regeneration of the sample occurs only partially, as the band gap is still shifted after 16 h of regeneration in CO_2 compared to oxidative conditions. Bare ceria is closest to a fully regenerated state, while the vanadia-loaded samples are more reduced.

Figure 1d depicts the peak area resulting from ceria and vanadia reduction for bare ceria and vanadia-loaded samples. The loading-dependent behavior of the reduction peak area is inverted to that of the band gap energy, further indicating that

the band gap energy behavior is caused by the significant intensity of the reduction peak, consistent with our previous results.[41] The reduction peak shows a strong intensity increase under reductive conditions for all samples (Figure 1a and b between 600–800 nm). Ceria exhibits the smallest increase, which is caused by the fact that ceria shows only $Ce^{3+} \rightarrow Ce^{4+}$ transitions, while vanadia is also subject to d-d transitions. More d-d transitions of vanadia are observed with increasing vanadia loading under H_2 conditions, leading to a generally higher intensity in the reduction region with increasing vanadia loading, indicating more reduced vanadia species. Under regenerative conditions, the reduction peak intensity of bare ceria significantly decreases significantly throughout the first hour and then slows down, leaving ceria partially reduced after 16 h, which indicates that Ce^{3+} states are still present in the ceria bulk. The 0.57 V/nm^2 sample shows a similar behavior as bare ceria, while the 1.36 V/nm^2 sample exhibits a more constant regeneration rate with a slower initial regeneration. The 2.83 V/nm^2 sample shows the most significant deviation from this behavior. For the first 30 minutes, a plateau in the reduction peak intensity is observed, which then decreases faster than for the other samples. After 16 h, bare ceria shows the lowest reduction peak intensity, while the other samples show an increasing intensity with increasing vanadia loading. However, the difference between the 0.57 and 1.36 V/nm^2 sample after 16 h is very small. The observed behavior after 16 h may indicate that either vanadia is reduced or that ceria is still reduced due to slowed bulk regeneration caused by the presence of vanadia. However, all samples are partially regenerated by CO_2, leading to a lower intensity of the reduction peak caused by a decrease in the number of Ce^{3+} and $V^{3+/4+}$ states.

To gain further insight into the subsurface/bulk re-oxidation of the samples and to differentiate between ceria and vanadia contributions, Vis-Raman spectroscopy (514 nm excitation) was performed under the same conditions. Figure 2 depicts in situ Vis-Raman spectra of bare ceria and ceria-loaded vanadia at a loading density of 1.36 V/nm^2 under oxidative, reductive and regenerative conditions at 550 °C. The changes in the F_{2g} position and the vanadyl area were quantified for all four samples and are given in Figure 2c and d, respectively. The corresponding in situ Vis-Raman spectra for the 0.57 and 2.83 V/nm^2 sample are given in the SI (see Figure S2). For clarity, the spectra recorded in 12.5% CO_2/He after 150 minutes are not shown.

As can be seen in Figure 2a, the intensity of the spectra decreases significantly under reductive conditions. The spectrum under oxidative conditions shows peaks at 245, 405, 455, 590, and 1170 cm^{-1}, which originate from the 2TA phonon, the transversal Ce–O surface phonon, the F_{2g} mode, the defect region (contributions from Ce^{3+} and oxygen vacancies), and the 2LO phonon, respectively.[32,62,63] Relevant spectral changes under reductive conditions (besides the general decrease in intensity) include the shift of the F_{2g} peak as an indicator for ceria reduction as well as the occurrence of a peak at 1064 cm^{-1}, which would be consistent with Ce–H bonds of bulk hydrides, indicating significant bulk reduction.[64] This reduction
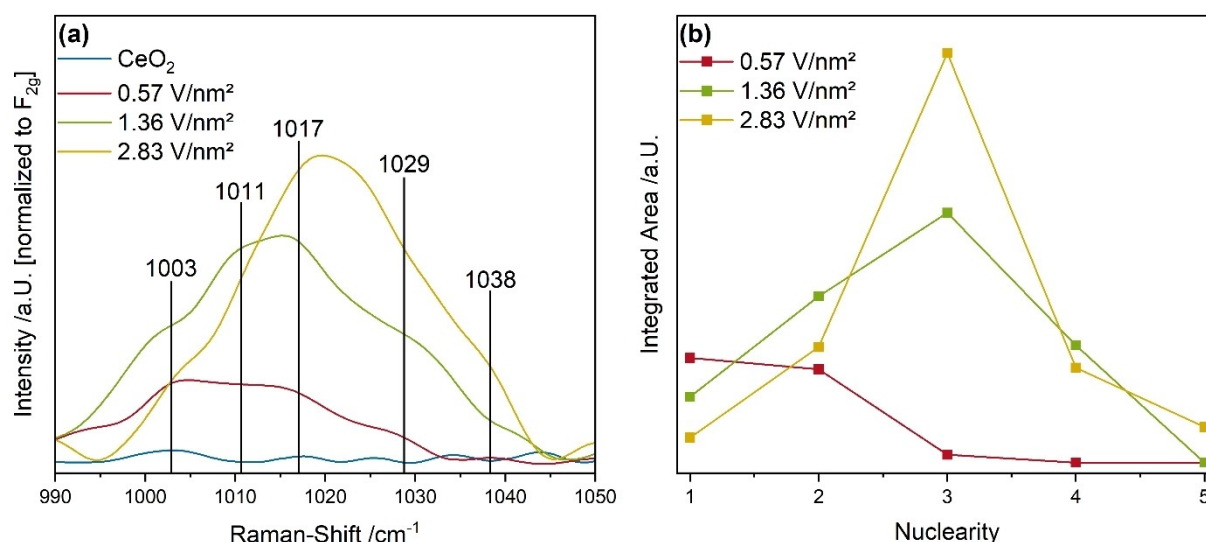
ChemCatChem

Research Article
doi.org/10.1002/cctc.202301409

Chemistry Europe
European Chemical
Societies Publishing

Figure 2. In situ Vis-Raman (514 nm excitation) spectra of **(a)** bare ceria and **(b)** the 1.36 V/nm^2 sample recorded under different gas feeds at 550 °C. The insets give an enlarged view of the region between 200 and 1300 cm^{-1}. Quantification of the **(c)** F_{2g} shift and **(d)** vanadyl peak. CeVO$_4$ was only detected for the 2.83 V/nm^2 sample (see Figure S2).

is still prominent after 16 h of regeneration with CO_2. While this peak position would also be consistent with the presence of carbonate, such an assignment can be safely ruled out, due its appearance during exposure to 7.5% H_2/Ar, that is, in the absence of CO_2.

The Vis-Raman spectra of the 1.36 V/nm^2 sample, shown in Figure 2b, are dominated by ceria contributions but additional peaks due to the presence of vanadia are located at 860, 920, and within the vanadyl region, the position of which varies depending on the loading (1008–1020 cm^{-1}). These signals are assigned to anchoring V–O–Ce, bridging V–O–V and terminal V=O bonds.[65] In addition, two peaks at 780 and 851 cm^{-1} are detected for the 2.83 V/nm^2 sample (see Figure S2b), which are indicative of CeVO$_4$ formation.[65,66] Due to the resonance enhancement of the vanadia species at 514 nm excitation (see Figure 1), a fine structure of the vanadyl peak can be observed in the Vis-Raman spectra, which will be discussed separately below (see Figure 3).[67] The F_{2g} and Ce–H peaks show a similar behaviour for the vanadia-loaded sample as for bare ceria. The vanadyl peak fully disappears under reducing conditions and gradually increases in intensity under regenerative conditions.

For detailed analysis, the F_{2g} red-shift and the vanadyl intensity were quantified (see Figure 2c and d). The red-shift of the F_{2g} peak is caused by the presence of Ce^{3+} ions in the lattice as a result of reduction, which distort the lattice due

to their larger diameter compared to Ce^{4+} ions.[54] Therefore, under reductive conditions, the F_{2g} mode of all four samples shows a significant red-shift. Ceria exhibits the smallest shift of ~2 cm^{-1}, while the red-shift increases with increasing vanadia loading up to 4 cm^{-1} for the 1.36 V/nm^2 sample, but then decreases again for the 2.83 V/nm^2 sample (2 cm^{-1}). During the first 30 minutes of regeneration, the F_{2g} peak shows a strong blue-shift for all samples, and then stays almost constant for the following 16 h. Overall, ceria seems to be fully re-oxidized in the subsurface when regenerated with CO_2, appearing even more oxidized than under O_2 atmosphere. A similar behavior is observed for the 2.83 V/nm^2 sample. The F_{2g} positions of the 0.57 and 1.36 V/nm^2 samples also recover significantly during the initial 30 minutes but then show a further continuous shift for 2 h, until a constant value is reached that is blue-shifted compared to the initial position. These differences in behaviour between the vanadia samples may originate from the different vanadia nuclearities, which have previously been shown to have loading-dependent functionalities.[41,53,65,67–69] A comparison of the UV-Vis and Vis-Raman spectroscopic results reveals differences regarding the re-oxidation behavior (see above). The fact that the F_{2g} peak returns to its initial position after 16 h, while the UV-Vis reduction peak area has only partially recovered, is likely caused by the increased 514 nm absorption of a partially reduced catalyst (see Figure 1), decreasing

ChemCatChem

Research Article
doi.org/10.1002/cctc.202301409

**Chemistry
Europe**
European Chemical
Societies Publishing

Figure 3. (a) Vanadyl fine structure from Raman spectra (514 nm excitation) of vanadia-loaded samples recorded during exposure to 12.5% O_2/He at 550 °C. The positions of the individual nuclearities are marked. (b) Nuclearity distribution of the vanadia-loaded samples based on a peak-fit analysis.
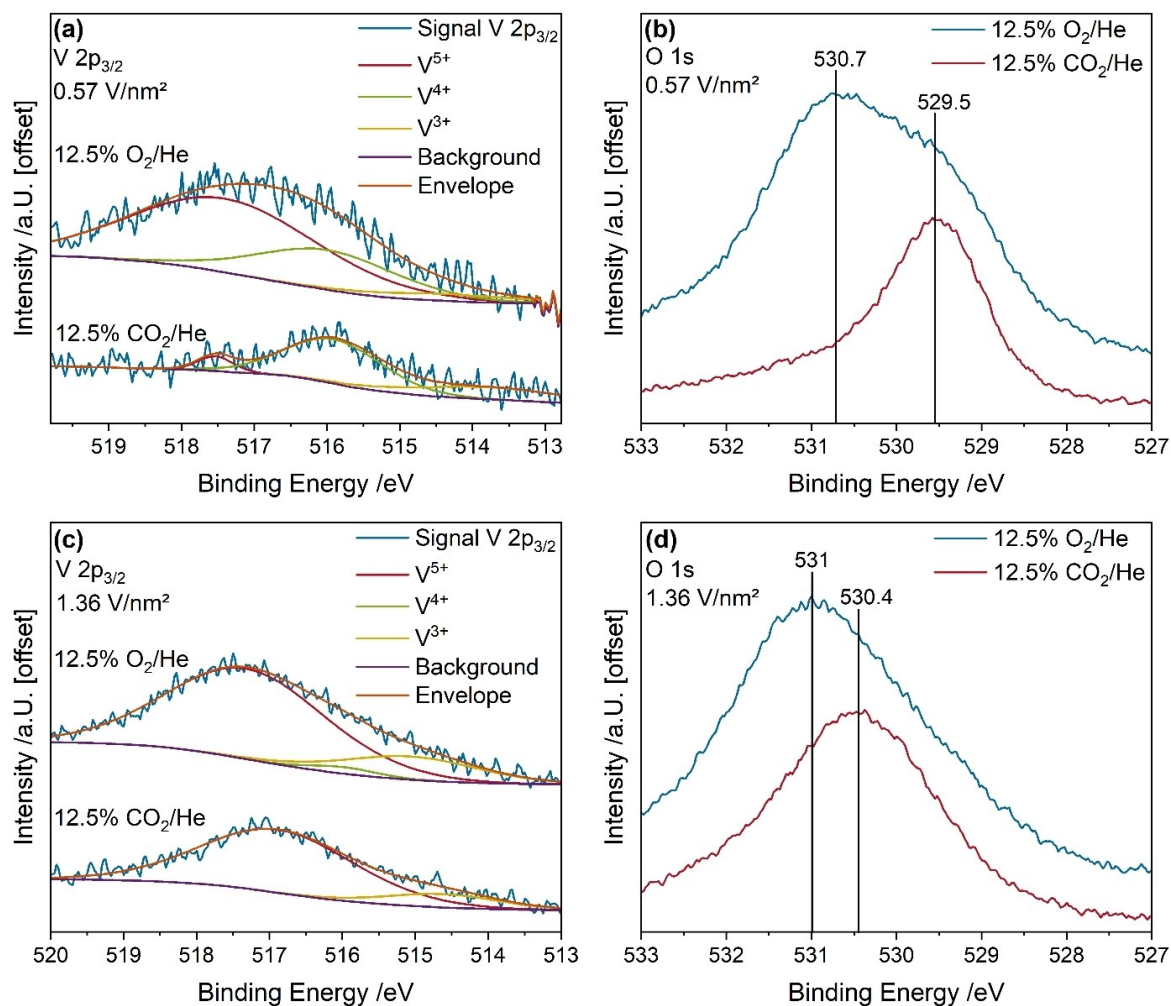
the information depth of Vis-Raman as compared to UV-Vis spectra.

Figure 2d shows the integrated areas of the vanadyl peak and of $CeVO_4$, which was only observed for the 2.83 V/nm² loading. The presence of $CeVO_4$ is expected as its formation is favored at high loadings, elevated temperatures and under reducing conditions.[52,65,66] The vanadyl peak almost fully disappears for all vanadia-loaded samples under reducing conditions. The V=O peaks of the 0.57 and 1.36 V/nm² samples barely regenerate for the first 2 h, while at the same time, ceria is strongly re-oxidized (see Figure 2c), indicating that the regeneration of the ceria bulk is favorable. Afterwards, the V=O peaks regenerate gradually, but even after 16 h, vanadia is still partially reduced. This behavior is more pronounced for the 0.57 V/nm² sample, while the vanadyl intensity of the 1.36 V/nm² sample almost fully recovers its initial intensity. The observed differences may be caused by the different surface compositions of the catalysts, as will be explored in more detail below (see Figures 3–5). For the 2.83 V/nm² sample, the vanadyl peak regenerates slowly. After 16 h, only 22% of the initial vanadyl area is regenerated. Additionally, a prominent $CeVO_4$ peak is observed, indicating the predominant formation of $CeVO_4$ during the regeneration process. The Raman results for the vanadia-loaded samples (see Figure 2d) are in good agreement with the UV-Vis results (see Figure 1d), as the reduction peak was observed to be more intense for vanadia-loaded samples than for bare ceria after 16 h. Vis-Raman spectra indicate that this difference originates to a significant degree from the presence of partially reduced vanadia. The slow regeneration of the 2.83 V/nm² sample, as observed by a decrease in UV-Vis reduction peak area, is likely caused by the delayed formation of $CeVO_4$, re-oxidizing the vanadia.

The vanadyl fine structure is used to quantify the nuclearity distribution of the surface vanadia species. To this end, Figure 3a depicts the vanadyl region of Vis-Raman spectra recorded at 514 nm excitation at 550 °C under 12.5% O_2/He

conditions compared to bare ceria. Figure 3b shows the nuclearity distribution as a function of vanadium loading based on a peak-fitting analysis (see Experimental Section). The marked positions in Figure 3a represent different nuclearities, whereby the positions may vary by ~1 cm⁻¹ as they depend on the exact structural environment. The fine structure is caused by dipole-dipole interactions between V=O groups of one species. The dipole-dipole interaction leads to a blue-shift of the V=O vibration, which increases the more vanadia, the larger the vanadia structures. This behavior allows the assignment of different chain lengths as already established in the literature.[41,53,67] For the vanadyl fine structure displayed in Figure 3a, peaks are observed at 1003, 1011, 1017, 1029, and 1038 cm⁻¹, which originate from the V=O stretching vibration of monomeric, dimeric, trimeric, tetrameric and oligomeric vanadia.[41,53,67] It is assumed that the nuclearity distribution may only be varied by sintering, for which there is no evidence.[70] Also, there has been no indication for gas-phase dependent changes in the nuclearity distribution.

According to Figure 3b, the vanadyl signal of the 0.57 V/nm² sample is dominated by monomeric and dimeric contributions, while the 1.36 and especially the 2.83 V/nm² samples display a sharp focus around trimeric species, which are (except for hexameric rings) the most stable nuclearity.[68,69] The number of monomeric vanadia species decreases with increasing vanadia loading while oligomeric species (nuclearities > 4) are most abundant on the 2.83 V/nm² sample. These differences in the nuclearity have previously been shown to result in a different reactivity behavior. For example, dimers and oligomers facilitate the hydrogen transfer and therefore catalyst reduction, while monomers can interact with surface oxygen vacancies.[53] Furthermore, ceria surface lattice oxygen in proximity to vanadia structures is more easily reduced than surface lattice oxygen of bare ceria. However, this effect depends on the nuclearity and is most pronounced for dimers and least for

ChemCatChem

Research Article
doi.org/10.1002/cctc.202301409

Chemistry Europe
European Chemical
Societies Publishing

Figure 4. Quasi in situ XP spectra of the V $2p_{3/2}$ regions of the **(a)** 0.57 V/nm^2 and **(c)** 1.36 V/nm^2 samples after pre-treatment under oxidative (12.5% O$_2$/He), reductive (7.5% H$_2$/Ar), and regenerative (12.5% CO$_2$/He) conditions at 550°C, subsequent cooling to room temperature in He, and inert transfer to the analysis chamber. Shown are spectra after oxidizing and regenerative conditions, together with the results of the fitting analysis of the vanadium signal. On the right, spectra of the corresponding O1s regions of the **(b)** 0.57 V/nm^2 and **(d)** 1.36 V/nm^2 samples are shown together with the peak maxima.
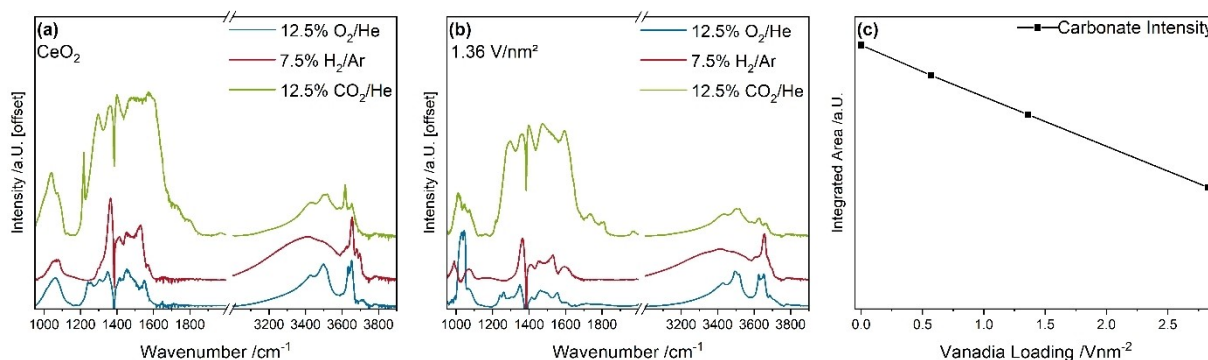
Figure 5. Quasi in situ DRIFT spectra of **(a)** bare ceria and **(b)** the 1.36 V/nm^2 sample recorded after exposure to the indicated gas feeds at 550°C and subsequent cooling to room temperature in He. **(c)** The carbonate area between 1200 and 1800 cm^{-1} was quantified based on the data recorded after oxidative conditions (12.5% CO$_2$/He). Spectra were offset for clarity.

trimers due to their high stability.[68,69] This explains the increased reduction of the 0.57 and 1.36 V/nm^2 samples (see Figure 2c) and the decreased reduction of the 2.83 V/nm^2 sample due to the abundant amount of stable trimers.

Furthermore, the re-oxidation of reduced vanadia species may also depend on the nuclearity. To this end, monomers were previously shown to interact with surface oxygen vacancies in their proximity.[41,65,68] While a facilitated recovery

ChemCatChem

Research Article
doi.org/10.1002/cctc.202301409

Chemistry
Europe
European Chemical
Societies Publishing

may be expected at elevated temperatures, fully/partially reduced monomers were recently shown not to be fully regenerated by ceria lattice oxygen or gas-phase CO_2 due to their thermodynamic stability.[71] However, since a fully oxidized dimer or trimer is thermodynamically significantly more stable than a monomer, full re-oxidation of these species might occur. This is evidenced by the regeneration of the vanadyl intensity (see Figure 2d), where the 0.57 V/nm² sample becomes only partially re-oxidized after 16 h but the 1.36 V/nm² sample is almost fully regenerated due to the presence of higher nuclearities. The 2.83 V/nm² sample cannot be directly compared to these samples due to the additional transformation of VO_x to $CeVO_4$.

To further investigate the nuclearity-dependent regeneration behavior, quasi in situ XP spectroscopy, that is, XP spectroscopy after different gas exposures without exposure to air, was applied to determine the vanadium oxidation state in the 0.57 and 1.36 V/nm² samples. Figure 4 shows the V $2p_{3/2}$ and O 1s photoemissions of the 0.57 and 1.36 V/nm² samples after a 30 min exposure to oxidative and regenerative conditions and subsequent transfer to the analysis chamber. The spectra of the V $2p_{3/2}$ region were fitted using three components (see Experimental Section), resulting in the distribution of vanadium oxidation states summarized in Table 1. Under oxidative conditions, the two samples show a very similar behavior and a higher oxidation state than under the same gas feed at 275 °C, as shown previously.[52] After reduction and subsequent re-oxidation of the samples, the V $2p_{3/2}$ photoemission regions of the two samples show significant differences, consistent with the previous proposition of a nuclearity-dependent re-oxidation behavior. For the following discussion, the amount of V^{5+} species during reductive conditions is assumed to be zero since V^{5+} species could not be observed in Vis-Raman spectra. For the 0.57 V/nm² sample, only a small amount of V^{5+} species is regenerated, while most species are present in the partially oxidized V^{4+} state, but V^{3+} species are also observed. This behavior is in very good agreement with previous DFT results on the regeneration of monomeric VO_x on CeO_2 using CO_2, where a re-oxidation from fully reduced to partially reduced was shown to be favored over full re-oxidation,[71] which is also visible from the reduced average oxidation state of 3.8 after regeneration (see Table 1). In contrast, the 1.36 V/nm² sample, due to the facilitated re-oxidation of higher nuclearities, is fully regenerated after 16 h, without significant difference in average oxidation state after

oxidative and regenerative gas treatments. Previously observed V^{4+} has possibly experienced disproportionation to V^{3+} and V^{5+}, which may explain the shifts in the relative contributions of each oxidation state (see Table 1). This further supports the presence of different re-oxidation pathways depending on vanadia nuclearity.[68,71] To emphasize that the low signal in the V $2p_{3/2}$ region is caused by the presence of vanadia, a comparison of all four samples under O_2 atmosphere based on the XP survey spectra is given in the SI (see Figure S3).

Figure 4b and d show the corresponding O 1s photoemission regions of the 0.57 and 1.36 V/nm² samples. The initial position of the maximum of the O 1s region at ~531 eV is in agreement with ceria bulk oxygen, but there may be small contributions from VO_x.[72,73] After reduction and re-oxidation, the O 1s peak of the 0.57 V/nm² sample shows a significant red-shift by 1.2 eV–529.5 eV, which was previously associated with the formation of defects interacting with lattice oxygen.[72–75] However, recent DFT calculations have shown the red-shift to originate from the formation of adsorbates, mainly Ce–OH and carbonates, rather than the presence of Ce^{3+}.[76] This effect is also observable for the 1.36 V/nm² sample but to a lesser extent, indicating that adsorbates might form during the regeneration process.

To gain further insight into the nature of the adsorbates, the O/Ce ratio was determined based on a fitting analysis of the Ce 3d and the O 1s photoemissions. From Table 2 it can be seen, that the amount of carbon on the surface increases significantly for both samples between the initial oxidizing and the regenerative conditions, as does the O/Ce ratio. Both findings are indicative of carbonate formation.

To identify adsorbates and to compare their surface concentrations DRIFT spectra were recorded. Figure 5 shows quasi in situ DRIFT spectra of bare ceria and ceria loaded with 1.36 V/nm² after exposure to 30 min of oxidative, reductive, and regenerative conditions at 550 °C. The changes observed in the carbonate region between 1200 and 1800 cm⁻¹ were quantified for all four samples (see Figure 5c). The quasi in situ DRIFT spectra for the 0.57 and 2.83 V/nm² samples are given in the SI (see Figure S4).

Figure 5a shows the quasi in situ DRIFT spectra of bare ceria. Between oxidative and regenerative conditions, a significant increase of the intensity in the region between 1200 and 1800 cm⁻¹ can be observed, where signals of carbon-based adsorbates (e.g. carbonates, formates) occur.[77–80] Besides, the formation of formates is confirmed by the appearance of a pronounced peak at ~2880 cm⁻¹ under CO_2 exposure (not

Table 1. Distribution of oxidation states of the 0.57 and 1.36 V/nm² samples after exposure to oxidative (12.5 % O_2/He) and regenerative (after reduction in 7.5 % H_2/Ar; 12.5 % CO_2/He) conditions based on a fitting analysis of the V $2p_{3/2}$ region (see Figure 4).

Sample	V^{5+}	V^{4+}	V^{3+}	Average
0.57 V/nm² O_2	0.68	0.27	0.05	4.63
0.57 V/nm² CO_2	0.08	0.64	0.28	3.80
1.36 V/nm² O_2	0.72	0.18	0.10	4.62
1.36 V/nm² CO_2	0.86	0.00	0.14	4.72

Table 2. Surface composition of the 0.57 and 1.36 V/nm² samples after exposure to oxidative (12.5 % O_2/He) and regenerative (after reduction in 7.5 % H_2/Ar; 12.5 % CO_2/He) conditions based on XPS analysis.

Sample	Ce 3d	O 1s	V $2p_{3/2}$	C 1s	O/Ce
0.57 V/nm² O_2	0.30	0.58	0.04	0.08	1.91
0.57 V/nm² CO_2	0.11	0.36	0.01	0.52	3.48
1.36 V/nm² O_2	0.25	0.61	0.04	0.10	2.54
1.36 V/nm² CO_2	0.16	0.49	0.04	0.31	3.11

ChemCatChem

Research Article
doi.org/10.1002/cctc.202301409

Chemistry
Europe
European Chemical
Societies Publishing

shown), which is accompanied by a decrease of Ce–OH signals between 3600 and 3700 cm^{-1}. Surface hydroxyl groups are likely consumed as water during the reduction and the corresponding sites may be re-oxidized by CO_2 to carbonates.[32] An increase in carbonates/formates is consistent with the XPS results discussed above and probably causes a partial deactivation of the ceria surface due to the high desorption barrier of CO after the lattice is regenerated.[71] For the 1.36 V/nm^2 sample (see Figure 5b), similar changes can be observed between the oxidative and regenerative gas phase. However, the intensity increase in the carbonate region is not as pronounced, which is explained by the presence of vanadia anchored to some of the surface lattice oxygen.[41,65] The carbonates are more likely to regenerate the ceria lattice first, before vanadia is regenerated by ceria due to oxygen spill-over.[71] This is in agreement with previous DFT studies, according to which ceria is the oxygen buffer that keeps vanadia oxidized to V^{5+}.[41,65,66,68] Direct oxidation of VO_x by CO_2 may proceed towards a partially oxidized state for monomers and a fully oxidized state for higher nuclearities, as discussed above.[68,69,71] However, based on the observed time delay between ceria and vanadia regeneration, oxygen spill-over seems to be the dominant path of regeneration, consistent with the finding from theory that ceria keeps vanadia in oxidation state $+V$.

Figure 5c shows the integrated carbonate signal for bare ceria and vanadia-loaded samples. A linear decrease in the carbonate area with increasing vanadia loading is observed, indicating that the anchoring of vanadia blocks surface lattice oxygen. Since ceria lattice oxygen is regenerated by CO_2 via carbonates[22,45,71] and the lattice subsequently re-oxidizes the VO_x, the time delay between ceria and vanadia re-oxidation can be readily explained (see Figures 1 and 2). The lower number of possible carbonate formation sites with higher vanadia loading also explains the differences in the F_{2g} blue-shift between bare ceria and the 0.57 and 1.36 V/nm^2 samples. There, ceria fully regenerates within the first 30 minutes, while the other two samples regenerate only partially over the first 30 minutes and then continue with their regeneration for 2 h in total (see Figure 2c). The 2.83 V/nm^2 sample is not fully comparable to these samples due to the formation of $CeVO_4$, which likely follows a different regeneration mechanism. However, the F_{2g} peak is still blue-shifted after regeneration compared to the initial oxidative conditions, indicating that the samples are more oxidized after reduction in H_2 and regeneration in CO_2 than under O_2/He exposure. In addition, the samples exhibit a partially reduced bulk after 16 h of regeneration (see Figure 1d).
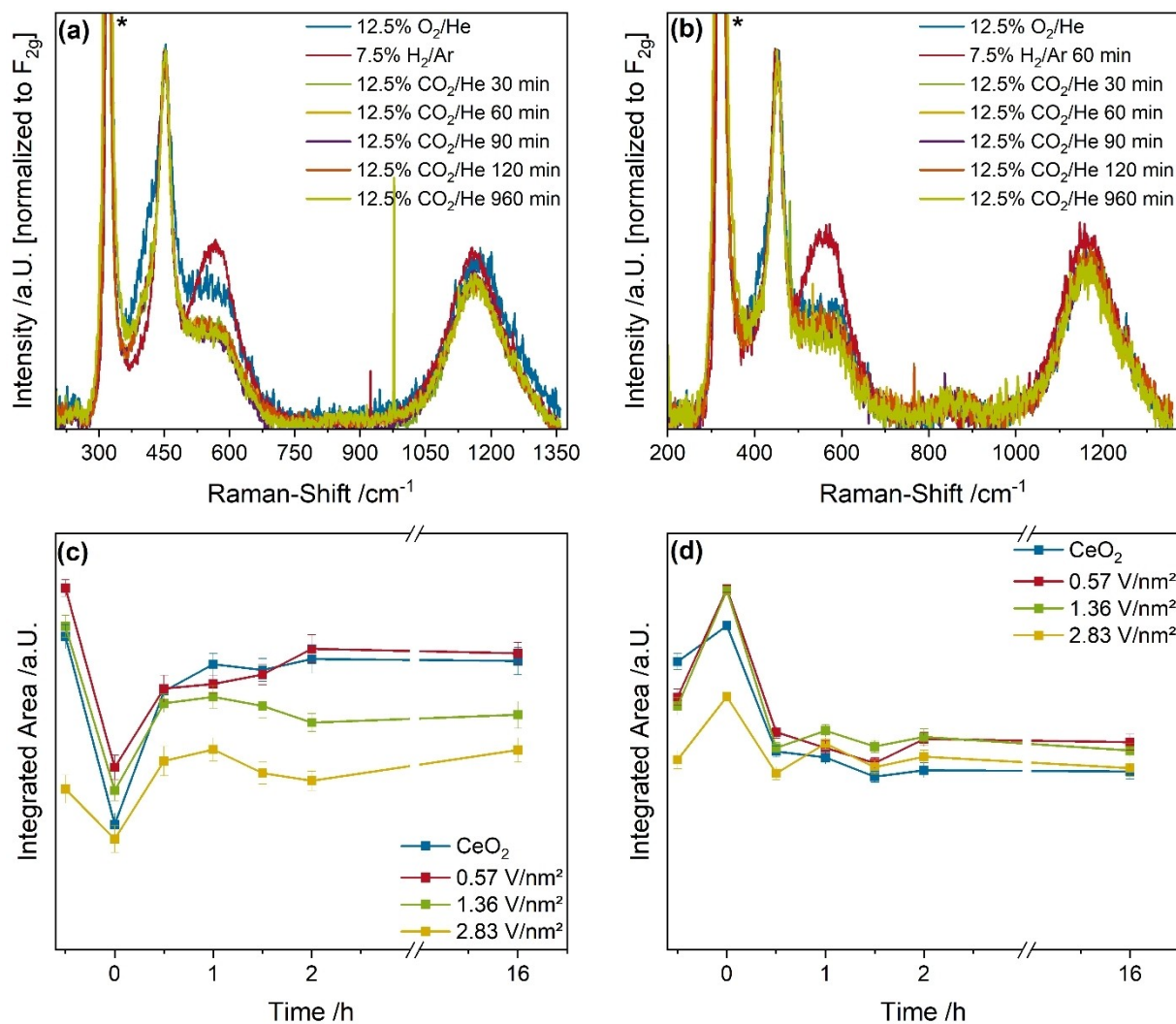
To investigate this phenomenon in more detail, UV-Raman spectra were recorded. Due to the high absorption of ceria at 385 nm, UV-Raman spectroscopy is selective to the ceria support, due to resonance effects at this wavelength, enabling the detailed investigation of the surface/subsurface region. Figure 6 shows in situ UV-Raman spectra of bare ceria and ceria loaded with 1.36 V/nm^2 under oxidative, reductive, and regenerative conditions after different exposure times. The changes observed in the spectra were quantified for all four samples and are summarized in Figure 4c and d, respectively. The corre-

sponding in situ UV-Raman spectra for the 0.57 and 2.83 V/nm^2 samples are given in the SI (see Figure S5). For clarity, the spectra recorded in 12.5% CO_2/He after 150 minutes are not shown.
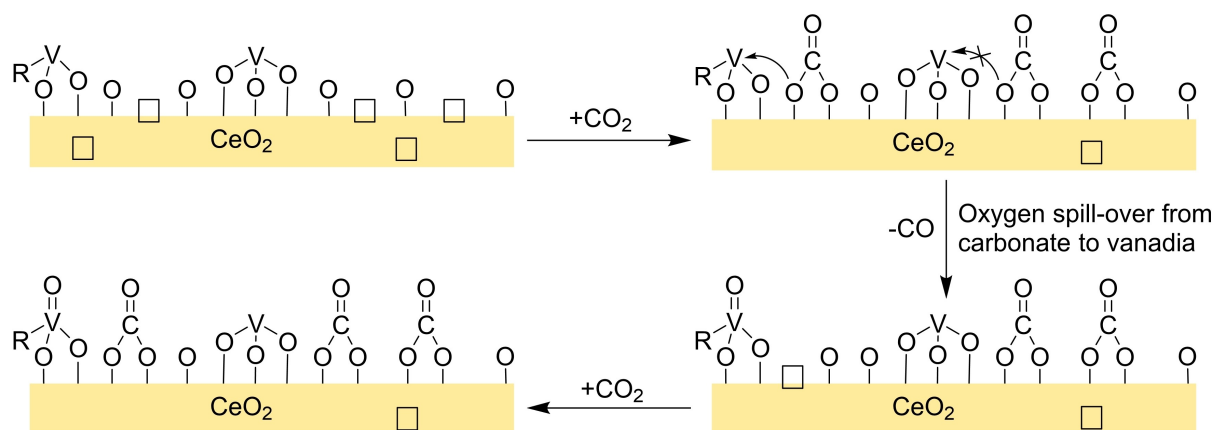
As shown in Figure 6a, the observed UV-Raman peaks for bare ceria resemble those observed in the Vis-Raman spectra (see Figure 2). However, due to the increased surface sensitivity and resonance enhancement, the transversal Ce–O surface phonon and the defect region of ceria is detected with significantly higher sensitivity,[41,62] allowing the surface oxygen dynamics to be discussed in more detail. The Ce–O surface phonon almost fully disappears upon switching from oxidative to reductive conditions and then gradually reappears during regeneration. In comparison, the intensity of the defect region first increases significantly during reductive conditions, as expected, and then decreases below its initial intensity during regenerative conditions. This is likely caused by CO_2-induced carbonate formation oxidizing previously existing as well as newly formed defects, thereby regenerating the surface to a higher degree than would be possible under O_2. The changes discussed for bare ceria are also observable for the vanadia-loaded samples (see Figures 6b and S4).

To quantify the changes observed in the UV-Raman spectra, a fitting analysis was performed (see Experimental Section). An exemplary fit for the 0.57 V/nm^2 sample under oxidizing, reductive, and regenerative conditions is shown in the SI (see Figure S6). The quantification results are summarized in Figure 6c and d for the topmost layer of ceria lattice oxygen and the defect region, respectively. The Ce–O surface phonon intensity first decreases for all samples under reductive conditions and then regenerates partially during CO_2 exposure, indicating that less Ce–O surface oxygen is present in the topmost ceria layer after regeneration. The initial reduction and regeneration is most significant for bare ceria and the 0.57 V/nm^2 sample and to a lower extent for the 1.36 and 2.83 V/nm^2 samples, as the number of surface Ce–O–Ce sites is reduced when vanadia is anchored to the support during impregnation.

The quantification of the defect region shows an intensity increase for all samples under reductive conditions (see Figure 6d), which is most pronounced for the 0.57 and 1.36 V/nm^2 samples. Most significantly, after 16 h, the defect intensity decreases below the intensity under oxidizing conditions for all samples, indicating that the samples are more oxidized after regeneration. Since at the same time the Ce–O surface phonon intensity decreases, this behavior can only be explained by the reaction of CO_2 to carbonate, consuming an oxygen vacancy. Such a process has no influence on the regeneration of Ce–O surface lattice oxygen (explaining the decrease) but consumes defect sites, thus oxidizing Ce^{3+} to Ce^{4+}, which results in a blue-shift of the F_{2g} mode (see Figure 2c). Since CO_2 can consume more vacancies than O_2, less Ce^{3+} states are present, leading to a blue-shift of the F_{2g} mode when compared to the oxidizing conditions, which makes the proposed re-oxidation process fully consistent with all spectroscopies performed in this study. Figure 7 summarizes the results in a mechanistic scheme.

ChemCatChem

Research Article
doi.org/10.1002/cctc.202301409

Chemistry
Europe

European Chemical
Societies Publishing

Figure 6. In situ UV-Raman (385 nm excitation) spectra of **(a)** bare ceria and **(b)** the 1.36 V/nm^2 sample recorded under different gas feeds at 550 °C, and quantification of **(c)** the transversal Ce–O surface phonon **(d)** the defect peak (see also Figure S5). For the latter the sum of both defect peaks was used.

Figure 7. Proposed mechanism for the activation of CO_2 and re-oxidation of reduced VO_x/CeO_2 catalysts.

ChemCatChem

Research Article
doi.org/10.1002/cctc.202301409

Chemistry Europe
European Chemical
Societies Publishing

3. Conclusions

In this study, we investigated the CO_2 activation and re-oxidation process of differently loaded VO_x/CeO_2 catalysts from a mechanistic point of view, thereby also establishing a basis for catalytic applications like CO_2-assisted ODH reactions. Multiple in situ methods including UV-Vis and multi-wavelength Raman spectroscopy, supported by quasi in situ DRIFTS and XPS, were used to elucidate both bulk and surface processes. Throughout the re-oxidation in CO_2 atmosphere for 16 h, in situ spectroscopy was continuously performed to gain insight into the time-dependent regeneration behavior.

After reduction and 16 h of regeneration using CO_2, the ceria bulk showed only partial re-oxidation. However, closer to the surface, regeneration seemed to be fully achieved for ceria, as the F_{2g} position indicated an even higher degree of oxidation after regeneration than under the initial O_2 conditions. Vanadia was regenerated on a slower time scale than ceria and could only be partially re-oxidized within the investigated timeframe.

The regeneration of ceria was determined to occur via carbonate formation on the reduced ceria surface, by adsorption of a CO_2 molecule into an oxygen vacancy. For bare ceria, this regeneration process could be observed via UV-Raman spectroscopy to occur on the topmost oxygen layer, where CO_2 can bind to defects. The resulting carbonates consume these defects but are stable enough to prevent CO desorption after regeneration.[71] This process consumes clean surface lattice oxygen of ceria as well as defect sites. The formation of surface carbonates was observed using DRIFTS, leading to seemingly more oxidized ceria than under O_2 conditions. This formation of surface carbonates was also observed for the vanadia-loaded samples but to a lesser extent, as vanadia is anchored to surface lattice oxygen, thereby blocking sites, leading to a slower regeneration of the ceria subsurface/bulk with increasing vanadia loading. Only the highest loaded sample deviated from that trend, as vanadia was transformed mostly to $CeVO_4$ during regeneration.

The samples showed a loading-dependent behavior. The regeneration of the VO_x/CeO_2 sample with the lowest vanadia loading was able to regenerate only partially and surface vanadium stayed in oxidation state V^{4+}, while the sample with medium loading showed an almost full regeneration of V^{5+} states. This behavior can be attributed to differences in the nuclearity distribution, which changes significantly with increasing vanadium surface density. The different nuclearities also influence the regeneration, as only a partial regeneration of monomeric vanadia species was predicted to be thermodynamically favorable.[71] However, higher nuclearities are thermodynamically more stable on ceria in their highest oxidized state, allowing for a full regeneration at higher vanadia loadings. Since the sample with the lowest vanadia loading is dominated by monomers, while higher loadings are dominated by the most stable trimers, the difference in the re-oxidation behavior can be readily explained.

The regeneration of the catalyst occurs mainly via the ceria lattice. The regeneration of vanadia can occur either by gas-phase CO_2 or by an oxygen spill-over from the ceria lattice. Due to the time delay between the ceria and vanadia regeneration, the oxygen spill-over pathway seems more likely and is in agreement with previous results according to which ceria keeps vanadium in oxidation state $+V$.

In summary, we present a comprehensive mechanistic study, which addresses the CO_2-based regeneration of differently-loaded and reduced VO_x/CeO_2 catalysts, by using multiple in situ spectroscopic methods. This approach enabled us to obtain a detailed understanding of the regeneration process on a molecular level using CO_2 as an oxidizing agent that will become a more relevant feed gas in chemical industry in the future. Our results can further serve as an experimental basis for understanding CO_2-assisted ODH reactions (ethylene, propane, etc.), which offer a green alternative to fossil fuel-based processes. Using vanadia-based catalysts, the nuclearity-dependent behavior might influence the catalytic performance significantly, while regeneration may become rate-determining when the catalysts are not sufficiently oxidized, leading to possible catalyst deactivation. The potential of our approach is illustrated for vanadia systems, but can readily be transferred to other important catalysts for CO_2-assisted ODH (e.g. supported indium oxide) or other processes that involve ceria-mediated CO_2 activation.

Supporting Information Summary

The supporting information contains additional in situ UV-Vis, Vis-Raman, UV-Raman, and DRIFTS data, as well as further information on the UV-Raman spectral analysis.

Conflict of Interests

The authors declare that they have no known competing financial interests or personal relationships that could have appeared to influence the work reported in this paper.

[1] T. J. Crowley, R. A. Berner, *Science* **2001**, *292*(5518), 870–872, DOI: 10.1126/science.1061664.

[2] F. M. Baena-Moreno, M. Rodríguez-Galán, F. Vega, B. Alonso-Fariñas, L. F. Vilches Arenas, B. Navarrete, *Energ. Sources A: Rec. Util. Environ. Effects* **2019**, *41*(12), 1403–1433, DOI: 10.1080/15567036.2018.1548518.

[3] A. Al-Mamoori, A. Krishnamurthy, A. A. Rownaghi, F. Rezaei, *Energy Technol.* **2017**, *5*(6), 834–849, DOI: 10.1002/ente.201600747.

[4] R. Chauvy, G. de Weireld, *Energy Technol.* **2020**, *8*(12), 1, DOI: 10.1002/ente.202000627.

[5] M. Aresta, A. Dibenedetto, A. Angelini, *J. CO2 Util.* **2013**, *3–4(14–15)*, 65–73, DOI: 10.1016/j.jcou.2013.08.001.

[6] E. Alper, O. Yuksel Orhan, *Petroleum* **2017**, *3*(1), 109–126, DOI: 10.1016/j.petlm.2016.11.003.

[7] D. S. Marlin, E. Sarron, Ó. Sigurbjörnsson, *Front. Chem.* **2018**, *6*, 446, DOI: 10.3389/fchem.2018.00446.

[8] Y. Gambo, S. Adamu, G. Tanimu, I. M. Abdullahi, R. A. Lucky, M. S. Ba-Shammakh, M. M. Hossain, *Appl. Catal. A: Gen.* **2021**, *623*, 118273, DOI: 10.1016/j.apcata.2021.118273.

[9] J. Baek, H. J. Yun, D. Yun, Y. Choi, J. Yi, *ACS Catal.* **2012**, *2*(9), 1893–1903, DOI: 10.1021/cs300198u.

[10] J. H. Carter, T. Bere, J. R. Pitchers, D. G. Hewes, B. D. Vandegehuchte, C. J. Kiely, S. H. Taylor, G. J. Hutchings, *Green Chem.* **2021**, *23*(24), 9747–9799, DOI: 10.1039/D1GC03700E.

[11] A. Álvarez, M. Borges, J. J. Corral-Pérez, J. G. Olcina, L. Hu, D. Cornu, R. Huang, D. Stoian, A. Urakawa, *ChemPhysChem* **2017**, *18*(22), 3135–3141, DOI: 10.1002/cphc.201700782.

[12] M. Jacquemin, A. Beuls, P. Ruiz, *Catal. Today* **2010**, *157*(1–4), 462–466, DOI: 10.1016/j.cattod.2010.06.016.

[13] C. Hess, *ChemPhysChem* **2009**, *10*(2), 319–326, DOI: 10.1002/cphc.200800585.

[14] I. E. Wachs, *Dalton Trans.* **2013**, *42*(33), 11762–11769, DOI: 10.1039/C3DT50692D.

[15] M. D. Argyle, K. Chen, A. T. Bell, E. Iglesia, *J. Catal.* **2002**, *208*(1), 139–149, DOI: 10.1006/jcat.2002.3570.

[16] B. Beck, M. Harth, N. G. Hamilton, C. Carrero, J. J. Uhlrich, A. Trunschke, S. Shaikhutdinov, H. Schubert, H.-J. Freund, R. Schlögl, J. Sauer, R. Schomäcker, *J. Catal.* **2012**, *296*, 120–131, DOI: 10.1016/j.jcat.2012.09.008.

[17] M. L. Balogun, S. Adamu, M. S. Ba-Shammakh, M. M. Hossain, *J. Industr. Eng. Chem.* **2021**, *96*(20), 82–97, DOI: 10.1016/j.jiec.2020.12.022.

[18] I. Ascoop, V. V. Galvita, K. Alexopoulos, M.-F. Reyniers, P. van der Voort, V. Bliznuk, G. B. Marin, *J. Catal.* **2016**, *335*, 1–10, DOI: 10.1016/j.jcat.2015.12.015.

[19] X. Jiang, B. M. Lis, S. C. Purdy, V. Paladugu, V. Fung, W. Quan, Z. Bao, W. Yang, Y. He, B. G. Sumpter, K. Page, I. E. Wachs, Z. Wu, *ACS Catal.* **2022**, *12*(18), 11239–11252, DOI: 10.1021/acscatal.2c02099.

[20] X. Jiang, B. M. Lis, Y. Wu, I. E. Wachs, Z. Wu, *J. Phys. Chem. C* **2023**, *127*(13), 6311–6320, DOI: 10.1021/acs.jpcc.3c00183.

[21] S. Rogg, C. Hess, *J. CO2 Util.* **2021**, *50*(9), 101604, DOI: 10.1016/j.jcou.2021.101604.

[22] A. Akah, M. Al-Ghrami, *Appl. Petrochem. Res.* **2015**, *5*(4), 377–392, DOI: 10.1007/s13203-015-0104-3.

[23] M. A. Botavina, G. Martra, Y. A. Agafonov, N. A. Gaidai, N. V. Nekrasov, D. V. Trushin, S. Coluccia, A. L. Lapidus, *Appl. Catal. A: Gen.* **2008**, *347*(2), 126–132, DOI: 10.1016/j.apcata.2008.05.037.

[24] F. Gashoul Daresibi, A. A. Khodadadi, Y. Mortazavi, S. Huotari, M. Ritala, *Mol. Catal.* **2022**, *526(80-–)*, 112396, DOI: 10.1016/j.mcat.2022.112396.

[25] P. Michorczyk, P. Pietrzyk, J. Ogonowski, *Microporous Mesoporous Mater.* **2012**, *161*, 56–66, DOI: 10.1016/j.micromeso.2012.05.011.

[26] H. Wang, T. D. Nguyen, G. Tsilomelekis, *Catal. Sci. Technol.* **2023**, *13*(8), 2360–2369, DOI: 10.1039/D2CY01563C.

[27] Z.-Y. Wang, Z.-H. He, L.-Y. Li, S.-Y. Yang, M.-X. He, Y.-C. Sun, K. Wang, J.-G. Chen, Z.-T. Liu, *Rare Met.* **2022**, *41*(7), 2129–2152, DOI: 10.1007/s12598-021-01959-y.

[28] C. A. Carrero, R. Schloegl, I. E. Wachs, R. Schomaecker, *ACS Catal.* **2014**, *4*(10), 3357–3380, DOI: 10.1021/cs5003417.

[29] A. Dinse, B. Frank, C. Hess, D. Habel, R. Schomäcker, *J. Mol. Catal A: Chem.* **2008**, *289*(1–2), 28–37, DOI: 10.1016/j.molcata.2008.04.007.

[30] H. Cordatos, D. Ford, R. J. Gorte, *J. Phys. Chem.* **1996**, *100*(46), 18128–18132, DOI: 10.1021/jp961110o.

[31] T. Duchoň, J. Hackl, D. N. Mueller, J. Kullgren, D. Du, S. D. Senanayake, C. Mouls, D. M. Gottlob, M. I. Khan, S. Cramm, K. Veltruská, V. Matolín, S. Nemšák, C. M. Schneider, *J. Mater. Chem. A* **2020**, *8*(11), 5501–5507, DOI: 10.1039/C9TA11784A.

[32] A. Filtschew, K. Hofmann, C. Hess, *J. Phys. Chem. C* **2016**, *120*(12), 6694–6703, DOI: 10.1021/acs.jpcc.6b00959.

[33] M. Ziemba, J. Weyel, C. Hess, *Appl. Catal. B: Environ.* **2022**, *301*, 120825, DOI: 10.1016/j.apcatb.2021.120825.

[34] Y. Liu, Z. Li, H. Xu, Y. Han, *Catal. Commun.* **2016**, *76*, 1–6, DOI: 10.1016/j.catcom.2015.12.011.

[35] E. M. Sala, N. Mazzanti, M. B. Mogensen, C. Chatzichristodoulou, *Solid State Ion.* **2022**, *375*(2), 115833, DOI: 10.1016/j.ssi.2021.115833.

[36] B. Ouyang, W. Tan, B. Liu, *Catal. Commun.* **2017**, *95*(3), 36–39, DOI: 10.1016/j.catcom.2017.03.005.

[37] J. Graciani, K. Mudiyanselage, F. Xu, A. E. Baber, J. Evans, S. D. Senanayake, D. J. Stacchiola, P. Liu, J. Hrbek, J. Fernández Sanz, J. A. Catalysis Rodriguez, *Science* **2014**, *345*(6196), 546–550, DOI: 10.1126/science.1253057.

[38] M. V. Martínez-Huerta, G. Deo, J. L. G. Fierro, M. A. Bañares, *J. Phys. Chem. C* **2007**, *111*(50), 18708–18714, DOI: 10.1021/jp0772225.

[39] A. Iglesias-Juez, M. V. Martínez-Huerta, E. Rojas-García, J.-M. Jehng, M. A. Bañares, *J. Phys. Chem. C* **2018**, *122*(2), 1197–1205, DOI: 10.1021/acs.jpcc.7b09832.

[40] W. Daniell, A. Ponchel, S. Kuba, F. Anderle, T. Weingand, D. H. Gregory, H. Knözinger, *Top. Catal.* **2002**, *20*(1/4), 65–74, DOI: 10.1023/A:1016399315511.

[41] L. Schumacher, C. Hess, *J. Catal.* **2021**, *398*(13), 29–43, DOI: 10.1016/j.jcat.2021.04.006.

[42] C. Karakaya, M. Kidder, C. Wolden, R. J. Kee, O. Deutschmann, *Ind. Eng. Chem. Res.* **2022**, *61*(39), 14482–14493, DOI: 10.1021/acs.iecr.2c02298.

[43] J. Dou, J. Funderburg, K. Yang, J. Liu, D. Chacko, K. Zhang, A. P. Harvey, V. P. Haribal, S. J. Zhou, F. Li, *ACS Catal.* **2023**, *13*(1), 213–223, DOI: 10.1021/acscatal.2c05286.

[44] M. L. Balogun, S. Adamu, I. A. Bakare, M. S. Ba-Shammakh, M. M. Hossain, *J. CO2 Util.* **2020**, *42*, 101329, DOI: 10.1016/j.jcou.2020.101329.

[45] T. Staudt, Y. Lykhach, N. Tsud, T. Skála, K. C. Prince, V. Matolín, J. Libuda, *J. Catal.* **2010**, *275*(1), 181–185, DOI: 10.1016/j.jcat.2010.07.032.

[46] P. S. Waleska, C. Hess, *J. Phys. Chem. C* **2016**, *120*(33), 18510–18519, DOI: 10.1021/acs.jpcc.6b01672.

[47] L. Antonov, D. Nedeltcheva, *Chem. Soc. Rev.* **2000**, *29*(3), 217–227, DOI: 10.1039/A900007K.

[48] C. Hess, *J. Catal.* **2007**, *248*(1), 120–123, DOI: 10.1016/j.jcat.2007.02.024.

[49] C. T. Nottbohm, C. Hess, *Catal. Commun.* **2012**, *22*, 39–42, DOI: 10.1016/j.catcom.2012.02.009.

[50] M. Ziemba, L. Schumacher, C. Hess, *J. Phys. Chem. Lett.* **2021**, *12*(15), 3749–3754, DOI: 10.1021/acs.jpclett.1c00892.

[51] P. Oelhafen, *J. Electr. Spectrosc. Rel. Phenom.* **1984**, *34*(2), 203, DOI: 10.1016/0368-2048(84)80044-4.

[52] L. Schumacher, M. Ziemba, K. Brunnengräber, L. Totzauer, K. Hofmann, B. J. M. Etzold, B. Albert, C. Hess, *J. Phys. Chem. C* **2023**, *127*(12), 5810–5824, DOI: 10.1021/acs.jpcc.3c00622.

[53] L. Schumacher, J. Weyel, C. Hess, *J. Am. Chem. Soc.* **2022**, *144*(32), 14874–14887, DOI: 10.1021/jacs.2c06303.

[54] C. Schilling, C. Hess, *J. Phys. Chem. C* **2018**, *122*(5), 2909–2917, DOI: 10.1021/acs.jpcc.8b00027.

[55] B. Huang, R. Gillen, J. Robertson, *J. Phys. Chem. C* **2014**, *118*(42), 24248–24256, DOI: 10.1021/jp506625h.

[56] P. Ober, S. Rogg, C. Hess, *ACS Catal.* **2020**, *10*(5), 2999–3008, DOI: 10.1021/acscatal.9b05174.

[57] C. Binet, A. Badri, J.-C. Lavalley, *J. Phys. Chem.* **1994**, *98*(25), 6392–6398, DOI: 10.1021/j100076a025.

[58] C. W. M. Castleton, J. Kullgren, K. Hermansson, *J. Chem. Phys.* **2007**, *127*(24), 244704, DOI: 10.1063/1.2800015.

[59] N. V. Skorodumova, R. Ahuja, S. I. Simak, I. A. Abrikosov, B. Johansson, B. I. Electronic Lundqvist, *Phys. Rev. B* **2001**, *64*(11), 548, DOI: 10.1103/PhysRevB.64.115108.

[60] D. Nitsche, C. Hess, *J. Phys. Chem. C* **2016**, *120*(2), 1025–1037, DOI: 10.1021/acs.jpcc.5b10317.

[61] B. Lamoureux, V. R. Singh, V. Jovic, J. Kuyyalil, T.-Y. Su, K. E. Smith, *Thin Solid Films* **2016**, *615*, 409–414, DOI: 10.1016/j.tsf.2016.07.062.

[62] C. Schilling, A. Hofmann, C. Hess, M. V. Ganduglia-Pirovano, *J. Phys. Chem. C* **2017**, *121*(38), 20834–20849, DOI: 10.1021/acs.jpcc.7b06643.

[63] W. H. Weber, K. C. Hass, J. R. McBride, *Phys. Rev. B* **1993**, *48*(1), 178–185, DOI: 10.1103/PhysRevB.48.178.

[64] Z. Li, K. Werner, L. Chen, A. Jia, K. Qian, J.-Q. Zhong, R. You, L. Wu, L. Zhang, H. Pan, X.-P. Wu, X.-Q. Gong, S. Shaikhutdinov, W. Huang, H.-J. Freund, *Chemistry* **2021**, *27*(16), 5268–5276, DOI: 10.1002/chem.202005374.

[65] Z. Wu, A. J. Rondinone, I. N. Ivanov, S. H. Overbury, *J. Phys. Chem. C* **2011**, *115*(51), 25368–25378, DOI: 10.1021/jp2084605.

[66] M. V. Martínez-Huerta, J. M. Coronado, M. Fernández-García, A. Iglesias-Juez, G. Deo, J. L. G. Fierro, M. A. Bañares, *J. Catal.* **2004**, *225*(1), 240–248, DOI: 10.1016/j.jcat.2004.04.005.

[67] M. Baron, H. Abbott, O. Bondarchuk, D. Stacchiola, A. Uhl, S. Shaikhutdinov, H.-J. Freund, C. Popa, M. V. Ganduglia-Pirovano, J. Sauer, *Angew. Chem. Int. Ed.* **2009**, *121*(43), 8150–8153, DOI: 10.1002/ange.200903085.

[68] C. Penschke, J. Paier, J. Sauer, *J. Phys. Chem. C* **2013**, *117*(10), 5274–5285, DOI: 10.1021/jp400520j.

[69] C. Penschke, J. Paier, J. Sauer, *J. Phys. Chem. C* **2018**, *122*(16), 9101–9110, DOI: 10.1021/acs.jpcc.8b01998.

[70] P. Granger, H. W. Siaka, S. B. Umbarkar, *Chem. Rec.* **2019**, *19*(9), 1813–1828, DOI: 10.1002/tcr.201800092, Published Online: Oct. 18, 2018.

[71] H.-X. Fan, L.-F. Zhen, A. Rajendran, J. Feng, W.-Y. Li, *Appl. Surf. Sci.* **2023**, *626*, 157250, DOI: 10.1016/j.apsusc.2023.157250.

[72] J. I. Flege, B. Kaemena, S. Gevers, F. Bertram, T. Wilkens, D. Bruns, J. Bätjer, T. Schmidt, J. Wollschläger, J. Falta, *Phys. Rev. B* **2011**, *84*(23), DOI: 10.1103/PhysRevB.84.235418.

[73] A. Allahgholi, J. I. Flege, S. Thieß, W. Drube, J. Falta, *ChemPhysChem* **2015**, *16*(5), 1083–1091, DOI: 10.1002/cphc.201402729, Published Online: Feb. 20, 2015.

[74] Y. Lykhach, V. Johánek, H. A. Aleksandrov, S. M. Kozlov, M. Happel, T. Skála, P. St. Petkov, N. Tsud, G. N. Vayssilov, K. C. Prince, K. M. Neyman, V. Matolín, J. Libuda, *J. Phys. Chem. C* **2012**, *116*(22), 12103–12113, DOI: 10.1021/jp302229x.

[75] M. M. Natile, A. Glisenti, *Surf. Sci. Spectra* **2006**, *13*(1), 17–30, DOI: 10.1116/11.20060401.

[76] N. Bosio, A. Schaefer, H. Grönbeck, *J. Phys. Condens. Matter* **2022**, *34*(17), DOI: 10.1088/1361-648X/ac4f7b, Published Online: Feb. 25, 2022.

[77] Z. Hu, Z. Wang, Y. Guo, L. Wang, *Environ. Sci. Technol*, DOI: 10.1021/acs.est.8b03448.

[78] F. C. Meunier, D. Tibiletti, A. Goguet, D. Reid, R. Burch, *Appl. Catal. A: Gen.* **2005**, *289*(1), 104–112, DOI: 10.1016/j.apcata.2005.04.018.

[79] T. Mokkelbost, I. Kaus, T. Grande, M.-A. Einarsrud, *Chem. Mater.* **2004**, *16*(25), 5489–5494, DOI: 10.1021/cm048583p.

[80] B. Wang, X. Wu, R. Ran, Z. Si, D. Weng, *J. Mol. Catal A: Chem.* **2012**, *356*, 100–105, DOI: 10.1016/j.molcata.2011.12.030.